Check for updates

Self-assembled Co$_{0.85}$Se/carbon nanowires as a highly effective and stable electrocatalyst for the hydrogen evolution reaction†

Baochen Sun, Xinqiang Wang,* Dongxu Yang* and Yuanfu Chen [ID] *

Self-assembled Co$_{0.85}$Se/carbon nanowires, constructed by Co$_{0.85}$Se nanoparticles homogenously embedded into carbon nanowires (Co$_{0.85}$Se@CNWs), have been synthesized through a facile solvothermal reaction and selenylation process. Compared to the bare Co$_{0.85}$Se NWs, the Co$_{0.85}$Se@CNW hybrid demonstrates high efficiency and stability for HER. It has a small Tafel slope of 43.4 mV dec^{-1}, a low onset potential of 138 mV *vs.* RHE, and a high cycling stability with more than 95% current retention after 1500 voltammetry cycles. The outstanding HER performance of Co$_{0.85}$Se@CNWs is attributed to its unique particle-in-nanowire architecture, which not only prevents the Co$_{0.85}$Se nanoparticles from aggregation, but also provides a highly conductive CNW matrix to promote the charge transfer in the electrocatalytic reaction, further enhancing the catalytic activity. This work provides a new strategy to rationally design transition metal-based selenide hybrids as highly effective and stable electrocatalysts for HER.

1. Introduction

With the advance of modern society, the global energy conjuncture is becoming ever more serious due to the consumption of fossil fuels. Therefore, searching for clean fuels to replace conventional fuels like coal and petroleum is crucial. Hydrogen can be obtained by the electrolysis of water. It has, therefore, immediately come to the fore of researchers' work due to its abundancy and high calorific value without causing pollution.[1–5] The hydrogen evolution reaction (HER) produces a lot of hydrogen through the energy-efficient method of electrolyzing water. Currently, it is well known that platinum is the best electrocatalyst for HER. Although platinum-based electrocatalysts show superior electrocatalytic activity and enduring stability, the high costs of platinum and its extreme rarity in the earth's crust limit the practical application of platinum-based electrocatalysts. Hence, this research has extraordinary significance in order to exploit highly efficient, low cost and stable non-precious electrocatalysts as replacements.[6]

Transition metal dichalcogenides (TMDs), for example MoSe$_2$,[7,50] MoS$_2$,[8–12] WSe$_2$,[13,14,49,51] and WS$_2$,[15,16] have shown high performance for HER. As one of the TMD series, cobalt selenides have been demonstrated as promising HER catalysts on account of their intrinsic high conductivity and excellent electrocatalytic properties. It is well known that cobalt mono- and diselenides have been widely investigated for the HER reaction. However, the electrocatalytic properties of Co$_{0.85}$Se have barely been reported and the HER activity of Co$_{0.85}$Se is far from satisfactory and still limited by the unreasonable structural design, lack of active sites and relatively low conductivity. Thus, the ration design and synthesis of a Co$_{0.85}$Se-based nanostructured electrocatalyst is important.

In order to synthesize high performance HER catalysts, two effective methods can be adopted. On the one hand, conductive carbon nanomaterials,[32] such as reduced graphene oxide (rGO),[17–20] metal–organic frameworks (MOFs)[21] and carbon nanotubes (CNTs)[22–26,37,52] can be incorporated to improve the HER performance of the electrocatalysts. It is expected that the nanostructured carbon materials enhance the conductivity and increase the active area of Co$_{0.85}$Se. Meanwhile, the carbon shell can protect Co$_{0.85}$Se from electrochemical corrosion in the electrocatalytic reaction, thus ensuring its long-term HER performance. On the other hand, by rationally designing the nanostructure of the catalysts into nanosheets,[28,48,49] nanocrystals,[33] nanowire arrays[34,35] or nanobelts,[36] more active sites will be obtained. Thus, in order to rationally design a Co$_{0.85}$Se-based nanostructured electrocatalyst, both approaches will be adopted to achieve good conductivity and abundant active sites, thus optimizing the HER performance.[27–30]

School of Electronic Science and Engineering, State Key Laboratory of Electronic Thin Films and Integrated Devices, University of Electronic Science and Technology of China, Chengdu 610054, PR China. E-mail: 843689677@qq.com; Dongxu_Y@hotmail.com; yfchen@uestc.edu.cn

Herein, we have synthesized a novel nanoparticle-embedded-nanowire architecture, which is constructed of $Co_{0.85}Se$ nanoparticles embedded into carbon nanowires ($Co_{0.85}Se@CNWs$) *via* a simple solvothermal method and selenylation process. Compared with the bare $Co_{0.85}Se$ nanowires ($Co_{0.85}Se$ NWs), the $Co_{0.85}Se@CNW$ hybrid delivers enhanced electrocatalytic performance. The $Co_{0.85}Se@CNW$ hybrid has a low onset potential of 138 mV (*vs.* RHE), a small Tafel slope of 43.4 mV dec^{-1} and a remarkable sustained cycling stability. The superior electrocatalytic capability benefits from its novel architecture that can afford plentiful reactive sites and guarantee the charge transfer in the electrocatalytic reaction.

2. Experimental

2.1 Synthesis of cobalt–NTA

The nitrilotriacetic acid (NTA) and $CoCl_2 \cdot H_2O$ were adopted as raw materials to synthesize cobalt–NTA. First of all, 1.9 g $CoCl_2 \cdot H_2O$ and 0.9 g NTA were dissolved into a solution of 15 mL of deionized water (DIW) and 45 mL of isopropyl alcohol. After that the precursor liquor was transferred into a 100 ml Teflon lined autoclave, and was resolved by a solvothermal process at 180 °C for 6 h. Finally, the specimen was repeatedly washed with deionized water and ethanol and dried at 60 °C for 12 h to obtain the cobalt–NTA.

2.2 Synthesis of $Co_{0.85}Se@CNWs$ and $Co_{0.85}Se$ NWs

0.3 g cobalt–NTA and 0.3 g glucose were put into 40 mL DIW and stirred for 30 min. After a solvothermal process at 180 °C for 12 h, the product was washed with ethanol and deionized water many times using a Nutsche filter and then dried at 60 °C. Then, the obtained powders were annealed at 650 °C for two hours, with a heating rate of 5 °C min^{-1} in order to obtain the Co@CNWs. Finally, amounts of the Co@CNWs powder and of the selenium powder were mixed and annealed at 650 °C for 2 h to obtain the $Co_{0.85}Se@CNWs$. The annealing process and selenization process for the $Co_{0.85}Se@CNWs$ is shown in Fig. S2.† The bare $Co_{0.85}Se$ NWs were synthesized in the same process apart from the addition of the glucose in the solvothermal reaction.

2.3 Characterizations

Scanning electron microscopy (SEM, JSM-7000F, and JEOL) and transmission electron microscopy (TEM, Tecnai F20 at 200 kV) were performed to examine the microstructures of $Co_{0.85}Se@CNWs$ and $Co_{0.85}Se$ NWs, respectively. The crystal structures of the $Co_{0.85}Se@CNW$ and $Co_{0.85}Se$ NW specimens were recorded by X-ray diffraction (XRD, Rigaku D/MAX-rA diffractometer). X-ray photoelectron spectroscopy (XPS, Kratos XSAM800 Al Kα Source Gun) was carried out to examine the chemical forms and compositions.

2.4 Electrochemical measurements

The electrochemical properties of the specimens were studied at an electrochemical station (CHI660C) using a three-electrode cell setup in an electrolyte (0.5 M H_2SO_4). 4 mg of $Co_{0.85}Se@CNWs$ was scattered in a mixed solvent of 750 μL of DIW and 250 μL of ethyl alcohol, and this was then sonicated for about 10 minutes to obtain a well-proportioned suspension. Subsequently, 50 μL of a Nafion D-520 dispersion (Alfa Aesar) was put in the solution and was sonicated for at least 30 min. Next, 10 μL of the above dispersion was dripped onto a glassy carbon electrode (GCE) (3 mm in diameter of a micropipette) to obtain the disparate working electrode (the catalyst loading was 0.283 mg cm^2). A saturated calomel electrode (SCE) was used as the reference electrode, and the counter electrode was a carbon electrode. In this work, the reference electrode was coordinated to the reversible hydrogen electrode (RHE), where $E_{RHE} = E_{SCE} + 0.254$ V. The linear sweep voltammetry (LSV) curves of the working electrode were measured at a scan rate of 5 mV s^{-1}. The electrochemical impedance spectra (EIS) were acquired at 0.2 V (*vs.* RHE) on the frequency scale of 0.1 Hz to 100 kHz, with an AC voltage of 5 mV. To study the stability of the $Co_{0.85}Se@CNWs$, it was studied with cyclic voltammetry (CV) with a scan rate of 100 mV s^{-1} from −0.346 V to 0.254 V (*vs.* RHE) for 1500 cycles and a time dependent current density (*i–t*) curve. In addition, the onset potential was identified using a current density of 1 mA cm^{-2}.

3. Results and discussion

First, a cobalt–nitrilotriacetic acid (NTA) nanowire precursor has been obtained by a solvothermal method (Fig. S1†). In the solvothermal process, the divalent metal ion Co^{2+} is anchored to carboxyl groups in the simplest unit of a chemical substance within NTA to take the preliminary shape of a one-dimensional long-chain cobalt–NTA coordination complex. The single polymer chain could self-assemble into nanowires and highly consistent nanostructures. Secondly, during the annealing process at 650 °C (Fig. S2†), the NTA is pyrolyzed into the low-density carbon nanowires, while the cobalt ions are reduced to metallic nanoparticles that are implanted into the carbon nanowires, thus the Co@CNWs have been obtained. In the subsequent selenization process (Fig. S2†), the Co nanoparticles that are embedded in the carbon nanowires react with Se and are converted to $Co_{0.85}Se$ nanoparticles, thus forming the $Co_{0.85}Se@CNWs$.

To analyze the crystal structures and the composition of the prepared samples, XRD was performed. According to Fig. 1a, the XRD spectra of the $Co_{0.85}Se@CNWs$ and $Co_{0.85}Se$ NWs have six diffraction peaks (33.26°, 44.73°, 50.56°, 60.38°, 61.86° and 69.91°), which correspond to the (101), (102), (110), (103), (112) and (202) planes of the standard hexagonal $Co_{0.85}Se$ (PDF card no. 52–1008), respectively.[45,53] To study the chemical composition of the $Co_{0.85}Se@CNWs$, analysis by XPS was carried out. The electron binding energy of Co 2p at 777.58 eV, 780.46 eV, 792.64 eV and 796.18 eV in the spectrum shown in Fig. 1b can be ascribed to Co^{3+} $2p_{3/2}$, Co^{2+} $2p_{3/2}$, Co^{3+} $2p_{1/2}$, and Co^{2+} $2p_{1/2}$ of $Co_{0.85}Se$.[38] The peaks at 782.86 eV and 802.12 eV can be attributed to the satellite peaks of Co^{3+} $2p_{3/2}$ and Co^{2+} $2p_{1/2}$, respectively. The results indicate that Co^{2+} and Co^{3+} coexist.[46,47] As shown in Fig. 1c, the peaks at 53.7 eV and 54.54 eV match with selenium $3d_{5/2}$ and $3d_{3/2}$ peaks, respectively, indicating the
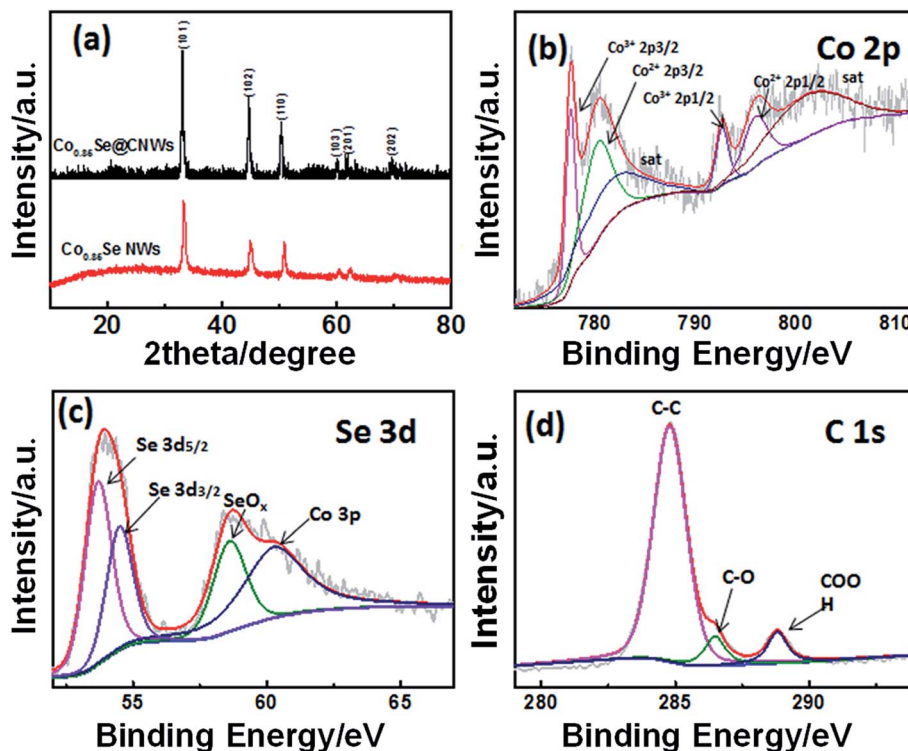
Fig. 1 (a) The XRD patterns of $Co_{0.85}Se@CNWs$ and $Co_{0.85}Se$ NWs. The high-resolution XPS spectra of (b) Co 2p, (c) Se 3d and (d) C 1 s for $Co_{0.85}Se@CNWs$.

constitution of the chemical bonds between cobalt and selenium.[27] The additional peak at the binding energy of 57–62 eV can be split into two peaks. The peak at 58.62 eV can be assigned to SeO_x, owing to the surface oxidation of Se,[46,47] and the peak at 60.3 eV coincides with Co 3p.[47] The XPS spectrum (Fig. 1d) shows that the C1s core level can be divided into three different peaks. Through analysis of the data, the dominating peak at 284.8 eV is attributed to the C–C bond. The 286.46 eV and 288.8 eV peaks identify the C–O and COOH groups, respectively.[44] The analysis of the XRD and XPS results confirms that the $Co_{0.85}Se@CNWs$ were properly synthesized.

In order to determine the micromorphological characteristics of the $Co_{0.85}Se@CNWs$ and the $Co_{0.85}Se$ NWs, scanning electron microscopy (SEM) was used. Fig. 2c and d are SEM images for the $Co_{0.85}Se@CNWs$. It is clear that the $Co_{0.85}Se@CNWs$ have a uniform linear structure, which is similar to the cobalt–NTA nanowires (Fig. S3†), indicating that the nanowire structure maintains its structure very well. However, compared with the $Co_{0.85}Se@CNWs$, the shape of the $Co_{0.85}Se$ NWs (Fig. 2a and b) is very uneven and the agglomeration and fracture phenomenon is severe. The SEM result demonstrates that the nanoparticle-embedded-nanowire architecture of $Co_{0.85}Se@CNWs$ can efficiently prevent the $Co_{0.85}Se$ nanoparticles from agglomeration and fracture during the annealing and selenization processes. Meanwhile, the BET specific surface area and pore size distribution of the $Co_{0.85}Se@CNWs$ have been measured. As displayed in Fig. S4a,† the $Co_{0.85}Se@CNWs$ present a large BET surface area of 60.91 m^2 g^{-1}, indicating its porous structure. The pore-size distribution (Fig. S4b†) further reveals that the $Co_{0.85}Se@CNWs$

possess clear macropores (6.91 nm and 6.71 nm). The porous structure of the $Co_{0.85}Se@CNWs$ can facilitate the access of electrolytes and provide sufficient pathways for electron transport during the HER process.

To further understand the detailed structure of $Co_{0.85}$-$Se@CNWs$, the microstructure of $Co_{0.85}Se@CNWs$ was characterized using transmission electron microscopy (TEM). Fig. 3a shows that the $Co_{0.85}Se@CNWs$ exhibit a uniform linear structure that is consistent with the SEM images. Fig. 3b shows the surface of the nanowires is rough and contains a large number of $Co_{0.85}Se$ nanoparticles, which are uniformly embedded in the carbon nanowires. The diameter of the $Co_{0.85}Se@CNWs$ was measured to be 150 nm. The enlarged image in Fig. 3c further reveals that the diameter of the $Co_{0.85}Se$ nanoparticles is approximately 23 nm. From the high-resolution TEM image (Fig. 3d), the interplanar spacings are measured to be 0.20 nm and 0.27 nm, corresponding to the spacing values of the (102) and (101) crystal planes of $Co_{0.85}Se$, respectively, and this is consistent with the XRD experimental data shown in Fig. 2a.[31] In order to confirm the uniform distribution of $Co_{0.85}Se$ nanoparticles in carbon nanowires, elemental mapping was measured by energy dispersive X-ray spectroscopy (EDX). Fig. 3f–i show the elemental (C, N, Co, and Se) mapping of a typical nanowire structure (Fig. 3e). The Co and Se element mapping patterns overlap adequately with the carbon element pattern, and this proves that the $Co_{0.85}Se$ nanoparticles are evenly distributed in the carbon nanowires. In addition, the nitrogen element in the $Co_{0.85}Se@CNWs$ is successfully doped during the pyrolyzation of NTA.
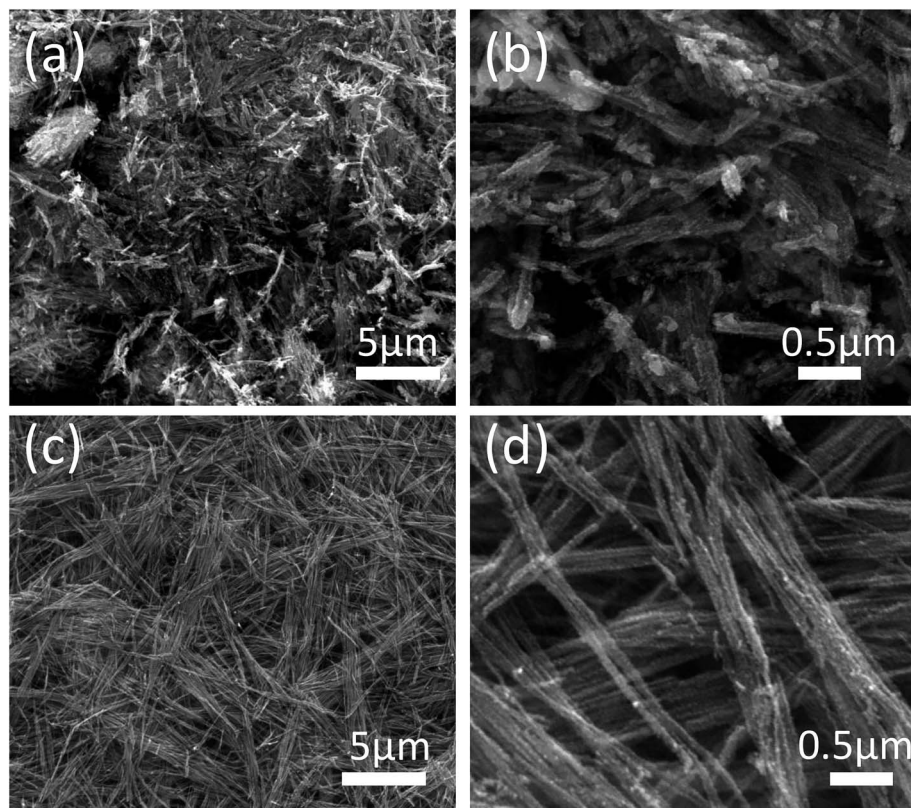
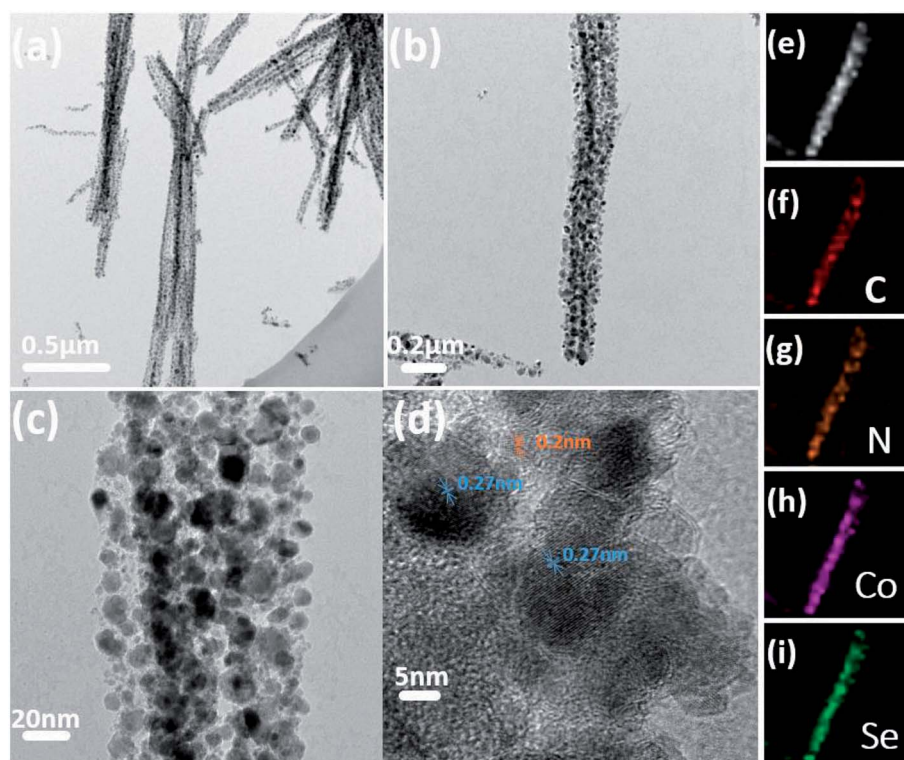Fig. 2   SEM images of (a and b) $Co_{0.85}Se$ NWs. SEM images of (c and d) $Co_{0.85}Se@CNWs$.

Fig. 3   (a, b and c) TEM and (d) HR-TEM images of $Co_{0.85}Se@CNWs$. (e) EDX mapping of an exclusive $Co_{0.85}Se@CNW$ confirms the presence of (f) C, (g) N, (h) Co, and (i) Se elements in the nanowires.

A highly efficient HER catalyst requires a large cathode current density at low potentials, as well as a high stability. In order to study the HER performance of the $Co_{0.85}Se@CNWs$ and the $Co_{0.85}Se$ NWS, electrochemical tests were carried out in an acid electrolyte (0.5 M H_2SO_4) using a standard three-electrode setup at room temperature. The LSV image (Fig. 4a) shows that under identical conditions, the onset potential of the $Co_{0.85}$-Se@CNWs (138 mV $vs.$ RHE) is distinctly lower than that of the $Co_{0.85}Se$ NWs (165 mV $vs.$ RHE). The polarization curve of the $Co_{0.85}Se@CNWs$ (32.7 mA cm^{-2} at -250 mV $vs.$ RHE) reveals a much higher current density than that of the $Co_{0.85}Se$ NWs (5.7 mA cm^{-2}). It was found that the Pt/C catalyst has the best electrochemical performance.[39,40] By studying the Tafel slope, it can be seen that the $Co_{0.85}Se@CNW$ (43.4 mV dec^{-1}) catalyst has a smaller Tafel slope. This can be compared with the $Co_{0.85}Se$ NW (58 mV dec^{-1}) catalyst, closely followed by the Pt/C (30 mV dec^{-1}) catalyst, as displayed in Fig. 4b. The results show that the $Co_{0.85}Se@CNW$ catalyst has excellent catalytic activity, and is much better than most previously reported Co- and Ni-based selenide electrocatalysts (Table S1†).

Generally, there are two mechanisms involved in the hydrogen evolution reaction.[16] These two mechanisms have a uniform initial step, in which the hydrated protons are absorbed onto the surface of the catalyst through the Volmer reaction process: $H_3O^+ + e \rightarrow H_{ads} + H_2O$. The next step, the Heyrovsky reaction, includes a hydronium bond and an electron transfer from the absorbed hydrogen atom ($H_3O^+ + H_{ads} + e \rightarrow H_2 + H_2O$). Another method for the second step is called the Tafel reaction, in which two absorbed hydrogen atoms are recombined ($H_{ads} + H_{ads} \rightarrow H_2$). Based on previous reports, the Tafel slopes of 120 mV dec^{-1}, 40 mV dec^{-1} and

30 mV dec^{-1} match those for the Volmer reaction, the Heyrovsky reaction and the Tafel reaction, respectively.[43,54] The Tafel slope for the $Co_{0.85}Se@CNWs$ is 43.4 mV dec^{-1}, therefore the Volmer–Heyrovsky mechanism plays a major role in this HER process.

The stability is also important for the electrocatalyst to be considered for pragmatic application. In order to investigate the stability of $Co_{0.85}Se@CNWs$ under electrocatalytic testing, cyclic voltammetry with a scan rate of 100 mV s^{-1} and a cycle number of 1500 was performed in an acid electrolyte (0.5 M H_2SO_4). As shown in Fig. 4c, the polarization curve after 1500 CV cycles is very close to that of the initial cycle, indicating that decay of the electrocatalyst is negligible. The morphology of the $Co_{0.85}Se@CNWs$ after the long-term HER stability test in acidic media has been characterized by SEM. As shown in Fig. S5,† there are almost no obvious changes in the morphology after the long-term HER test, confirming the good stability of the $Co_{0.85}Se@CNWs$ during the long-term electrochemical process. To further evaluate the stability of the $Co_{0.85}Se@CNWs$, its current density curve over time (Fig. 4d) was measured. The catalytic reaction was continued without interruption at a constant overpotential (0.2 V $vs.$ RHE) for 18 h in an acid electrolyte (0.5 M H_2SO_4). As shown in Fig. S6,† which shows a hackle-like current curve, the heightened vertical readings illustrate the alternating accumulation and release of bubbles during the reaction.[42]

In order to discover the reason for the enhanced catalytic performance of the $Co_{0.85}Se@CNWs$ compared to the bare $Co_{0.85}Se$ NWs, the double-layer capacitance (C_{dl}) was tested by a cyclic voltammetry technique to estimate a superficial area of the electrochemical.[41] At diverse scan rates of 20–
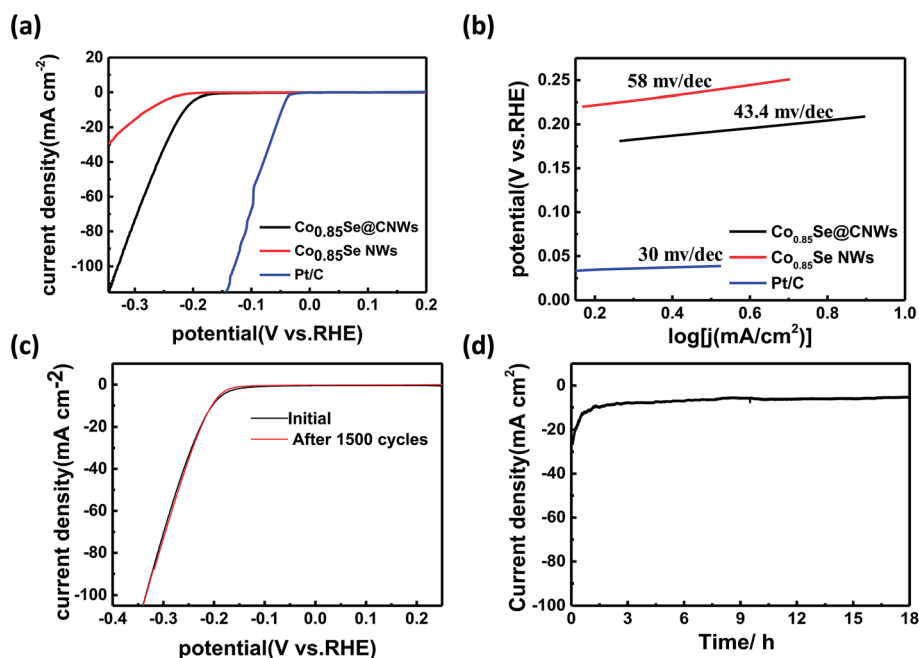

Fig. 4 Electrochemical performance of $Co_{0.85}Se@CNWs$ and $Co_{0.85}Se$ NWs. (a) Polarization curves of $Co_{0.85}Se@CNWs$, $Co_{0.85}Se$ NWs and the Pt/C catalyst recorded at a scan rate of 5 mV s^{-1} for HER. (b) Corresponding Tafel plots of $Co_{0.85}Se@CNWs$, $Co_{0.85}Se$ NWs and the Pt/C catalyst. (c) Polarization curves of $Co_{0.85}Se@CNWs$ before and after 1500 CV cycles at room temperature as a stability test. (d) Time dependence of current density under a static potential of 0.2 V $vs.$ RHE for $Co_{0.85}Se@CNWs$.
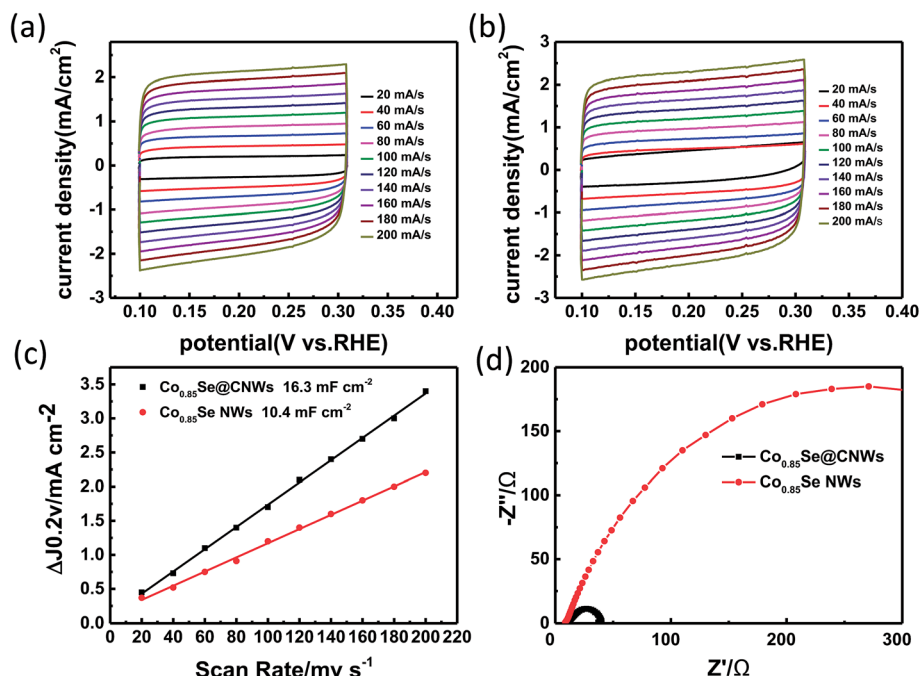
Fig. 5 Voltammograms of (a) $Co_{0.85}Se@CNWs$ and (b) $Co_{0.85}Se$ NWs. (c) Estimated C_{dl} of $Co_{0.85}Se@CNWs$ and $Co_{0.85}Se$ NWs. (d) Nyquist plots (100 kHz to 100 mHz) of $Co_{0.85}Se@CNWs$ and $Co_{0.85}Se$ NWs, performed at 0.2 V (*vs.* RHE).

200 mV s^{-1}, cyclic voltammetry was performed over the potential range of 0.1 to 0.3 V (*vs.* RHE). Fig. 5a and b show the voltammograms of the $Co_{0.85}Se@CNWs$ and of the $Co_{0.85}Se$ NWs, respectively. From these results, half of the difference between the positive and negative current densities ($\Delta J = J_{anodic} - J_{cathodic}$) at the potential of 0.2 V (*vs.* RHE) can be plotted as the CV scan rate, and the curves can be fit as a linear function. It can be clearly seen from Fig. 5c that the C_{dl} quantitative values of the $Co_{0.85}Se@CNWs$ and the $Co_{0.85}Se$ NWs are 16.3 mF cm^{-2} and 10.4 mF cm^{-2}, respectively. The above analysis indicates that the $Co_{0.85}Se@CNW$ catalyst has a sizeable active surface area and a substantial mass of active sites compared to the $Co_{0.85}Se$ NW catalyst. In addition, the electrode kinetics for the HER process was studied using electrochemical impedance spectroscopy (EIS). The Nyquist plots and equivalent circuit for the $Co_{0.85}Se@CNWs$ and $Co_{0.85}Se$ NWs is shown in Fig. 5d and S7,† respectively. The charge transfer resistances (R_{ct}) for the $Co_{0.85}Se@CNWs$ and $Co_{0.85}Se$ NWs are 39 Ω and 508 Ω, respectively. The small R_{ct} numerical value for the $Co_{0.85}Se@CNW$ catalyst indicates that it has faster kinetic properties, compared to the $Co_{0.85}Se$ NW catalyst.

As described above, the first-class HER property of $Co_{0.85}Se@CNWs$ is mainly due to several major factors. First of all, since $Co_{0.85}Se$ has an intrinsic semi-metal property, it has a high conductivity, which is advantageous for increasing the efficiency of the charge transfer. Secondly, the outstanding HER property of the $Co_{0.85}Se@CNW$ catalyst is attributed to its characteristic particle-in-nanowire architecture, which can prevent $Co_{0.85}Se$ nanoparticles from aggregation and afford abundant reactive sites, leading to high

catalytic activity. Moreover, the carbon shell can protect $Co_{0.85}Se$ from electrochemical corrosion in the electrocatalytic reaction, thus ensuring its long-term HER performance.

4. Conclusions

In summary, a $Co_{0.85}Se@CNW$ catalyst was synthesized by simple solvothermal and subsequent selenization processes. The $Co_{0.85}Se@CNW$ catalyst has favorable performance in acidic electrolyte. Compared with $Co_{0.85}Se$ NWs, the $Co_{0.85}Se@CNWs$ demonstrate superior efficiency and remarkable stability in the HER reaction. It has a small Tafel slope (43.4 mV dec^{-1}) and a low onset potential (138 mV *vs.* RHE). Meanwhile, a superior cycling stability with more than 95% high current retention is achieved after being tested over 1500 voltammetry cycles. The superior electrocatalytic performance is due to its unique architecture that can afford plentiful reactive sites and guarantee the charge transfer in the electrocatalytic reaction. The $Co_{0.85}Se@CNW$ catalyst is expected to be a highly efficient non-precious metal catalyst with remarkable performance and a low synthetic cost.

5. Experimental section

Further experimental details and characterizations and other relevant measurements for the electrocatalytic properties are offered in the ESI.†

Conflicts of interest

There are no conflicts to declare.

Acknowledgements

References

1 M. Gao, J. Liang, Y. Zheng, Y. Xu, J. Jiang, Q. Gao, J. Li and S. Yu, *Nat. Commun.*, 2015, **6**, 5982.

2 N. S. Lewis and D. G. Nocera, Energy utilization, *Proc. Natl. Acad. Sci. U. S. A.*, 2007, **104**, 20142.

3 L. R. Meza, S. Das and J. R. Greer, *Science*, 2014, **345**, 1322–1326.

4 J. He, Q. Li, Y. Chen, C. Xu, K. Zhou, X. Wang, W. Zhang and Y. Li, *Carbon*, 2017, **114**, 111–116.

5 J. He, K. Zhou, Y. Chen, C. Xu, J. Lin and W. Zhang, *Mater. Today Energy*, 2016, **1–2**, 11–16.

6 M. S. Faber and S. Jin, *Energy Environ. Sci.*, 2014, **7**, 3519–3542.

7 H. Tang, K. Dou, C. Kaun, Q. Kuang and S. Yang, *J. Mater. Chem. A*, 2014, **2**, 360–364.

8 T. F. Jaramillo, K. P. Jorgensen, J. Bonde, J. H. Nielsen, S. Horch and I. Chorkendorff, *Science*, 2007, **317**, 100–102.

9 L. Jia, X. Sun, Y. Jiang, S. Yu and C. Wang, *Adv. Funct. Mater.*, 2015, **25**, 1814–1820.

10 S. J. Rowley-Neale, D. A. Brownson, G. C. Smith, D. A. Sawtell, P. J. Kelly and C. E. Banks, *Nanoscale*, 2015, **7**, 18152–18168.

11 J. He, P. Li, W. Lv, K. Wen, Y. Chen, W. Zhang, Y. Li, W. Qin and W. He, *Electrochim. Acta*, 2016, **215**, 12–18.

12 J. He, Y. Chen, W. Lv, K. Wen, C. Xu, W. Zhang, Y. Li, W. Qin and W. He, *ACS Nano*, 2016, **10**, 10981–10987.

13 X. Wang, Y. Chen, B. Zheng, F. Qi, J. He, P. Li and W. Zhang, *Electrochim. Acta*, 2016, **222**, 1293–1299.

14 X. Wang, Y. Chen, B. Zheng, F. Qi, J. He, Q. Li, P. Li and W. Zhang, *J. Alloys Compd.*, 2017, **691**, 698–704.

15 F. Qi, P. Li, Y. Chen, B. Zheng, J. Liu, J. Zhou, J. He, X. Hao and W. Zhang, *Int. J. Hydrogen Energy*, 2017, **42**, 7811–7819.

16 X. Chia, A. Y. S. Eng, A. Ambrosi, S. M. Tan and M. Pumera, *Chem. Rev.*, 2015, **115**, 11941–11966.

17 L. Jia, X. Sun, Y. Jiang, S. Yu and C. Wang, *Adv. Funct. Mater.*, 2015, **25**, 1814–1820.

18 G. Huang, H. Liu, S. Wang, X. Yang, B. Liu, H. Chen and M. Xu, *J. Mater. Chem. A*, 2015, **3**, 24128–24138.

19 J. He, Y. Chen, W. Lv, K. Wen, Z. Wang, W. Zhang, Y. Li, W. Qin and W. He, *ACS Nano*, 2016, **10**, 8837–8842.

20 J. He, Y. Chen, W. Lv, K. Wen, P. Li, F. Qi, Z. Wang, W. Zhang, Y. Li, W. Qin and W. He, *J. Power Sources*, 2016, **327**, 474–480.

21 B. Nohra, H. El Moll, L. M. Rodriguez Albelo, P. Mialane, J. Marrot, C. Mellot-Draznieks, M. O. Keeffe, R. Ngo Biboum, J. Lemaire, B. Keita, L. Nadjo and A. Dolbecq, *J. Am. Chem. Soc.*, 2011, **133**, 13363–13374.

22 Y. Yan, X. Ge, Z. Liu, J. Wang, J. Lee and X. Wang, *Nanoscale*, 2013, **5**, 7768.

23 Y. Huang, H. Lu, H. Gu, J. Fu, S. Mo, C. Wei, Y. Miao and T. Liu, *Nanoscale*, 2015, **7**, 18595–18602.

24 X. Wang, Y. Chen, F. Qi, B. Zheng, J. He, Q. Li, P. Li, W. Zhang and Y. Li, *Electrochem. Commun.*, 2016, **72**, 74–78.

25 J. He, Y. Chen, W. Lv, K. Wen, C. Xu, W. Zhang, W. Qin and W. He, *ACS Energy Lett.*, 2016, **1**, 820–826.

26 J. He, Y. Chen, W. Lv, K. Wen, P. Li, Z. Wang, W. Zhang, W. Qin and W. He, *ACS Energy Lett.*, 2016, **1**, 16–20.

27 D. Kong, H. Wang, Z. Lu and Y. Cui, *J. Am. Chem. Soc.*, 2014, **136**, 4897–4900.

28 F. Wang, T. A. Shifa, X. Zhan, Y. Huang, K. Liu, Z. Cheng, C. Jiang and J. He, *Nanoscale*, 2015, **7**, 19764–19788.

29 Q. Liu, J. Shi, J. Hu, A. M. Asiri, Y. Luo and X. Sun, *ACS Appl. Mater. Interfaces*, 2015, **7**, 3877–3881.

30 J. He, Y. Chen, P. Li, F. Fu, Z. Wang and W. Zhang, *Electrochim. Acta*, 2015, **182**, 424–429.

31 H. Zhang, B. Yang, X. Wu, Z. Li, L. Lei and X. Zhang, *ACS Appl. Mater. Interfaces*, 2015, **7**, 1772–1779.

32 Y. Liu, H. Cheng, M. Lyu, S. Fan, Q. Liu, W. Zhang, Y. Zhi, C. Wang, C. Xiao, S. Wei, B. Ye and Y. Xie, *J. Am. Chem. Soc.*, 2014, **136**, 15670–15675.

33 I. H. Kwak, H. S. Im, D. M. Jang, Y. W. Kim, K. Park, Y. R. Lim, E. H. Cha and J. Park, *ACS Appl. Mater. Interfaces*, 2016, **8**, 5327–5334.

34 K. Liu, F. Wang, K. Xu, T. A. Shifa, Z. Cheng, X. Zhan and J. He, *Nanoscale*, 2016, **8**, 4699–4704.

35 W. Zhou, J. Lu, K. Zhou, L. Yang, Y. Ke, Z. Tang and S. Chen, *Nano Energy*, 2016, **28**, 143–150.

36 M. Gao, X. Cao, Q. Gao, Y. Xu, Y. Zheng, J. Jiang and S. Yu, *ACS Nano*, 2014, **8**, 3970–3978.

37 J. He, Y. Chen, P. Li, F. Fu, Z. Wang and W. Zhang, *J. Mater. Chem. A*, 2015, **3**, 18605–18610.

38 J. Yang, G. H. Cheng, J. H. Zeng, S. H. Yu, X. M. Liu and Y. T. Qian, *Chem. Mater.*, 2001, **13**, 848–853.

39 A. B. Laursen, S. Kegnaes, S. Dahl and I. Chorkendorff, *Energy Environ. Sci.*, 2012, **5**, 5577–5591.

40 M. B. Stevens, L. J. Enman, A. S. Batchellor, M. R. Cosby, A. E. Vise, C. D. M. Trang and S. W. Boettcher, *Chem. Mater.*, 2016, **29**, 120–140.

41 F. Qi, X. Wang, B. Zheng, Y. Chen, B. Yu, J. Zhou, J. He, P. Li, W. Zhang and Y. Li, *Electrochim. Acta*, 2017, **224**, 593–599.

42 S. Mao, Z. Wen, S. Ci, X. Guo, K. K. Ostrikov and J. Chen, *Small*, 2015, **11**, 414–419.

43 L. Liao, S. Wang, J. Xiao, X. Bian, Y. Zhang, M. D. Scanlon, X. Hu, Y. Tang, B. Liu and H. H. Girault, *Energy Environ. Sci.*, 2017, **7**, 387–392.

44 F. Zhang, J. Zhu, D. Zhang, U. Schwingenschlögl and H. N. Alshareef, *Nano Lett.*, 2017, **17**, 1302–1311.

45 Y. Yao, H. Chao, T. Chou, S. H. Chang, C. Wu, Y. Ling and J. Chang, *Sol. Energy*, 2016, **137**, 401–408.

46 B. Yu, F. Qi, X. Wang, B. Zheng, W. Hou, Y. Hu, J. Lin, W. Zhang, Y. Li and Y. Chen, *Electrochim. Acta*, 2017, **247**, 468–474.

47 B. Yu, F. Qi, Y. Chen, X. Wang, B. Zheng, W. Zhang, Y. Li and L. Zhang, *ACS Appl. Mater. Interfaces*, 2017, **9**, 30703–30710.

48 X. Wang, J. He, B. Zheng, W. Zhang and Y. Chen, *Electrochim. Acta*, 2018, **283**, 1660–1667.

49 X. Wang, Y. Chen, B. Zheng, F. Qi, J. He, P. Li and W. Zhang, *Electrochim. Acta*, 2016, **222**, 1293–1299.
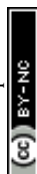
50 X. Wang, B. Zheng, B. Yu, B. Wang, W. Hou, W. Zhang and Y. Chen, *J. Mater. Chem. A*, 2018, **6**, 7842–7850.

51 X. Wang, Y. Chen, F. Qi, B. Zheng, J. He, Q. Li, P. Li, W. Zhang and Y. Li, *Electrochem. Commun.*, 2016, **72**, 74–78.

52 Y. Hu, B. Yu, W. Li, M. Ramadoss and Y. Chen, *Nanoscale*, 2019, **11**, 4876–4884.

53 Y. Huang, Z. Ma, Y. Hu, D. Chai, Y. Qiu, G. Gao and P. Hu, *RSC Adv.*, 2016, **6**, 51725.

54 B. Zheng, Y. Chen, F. Qi, X. Wang, W. Zhang, Y. Li and X. Li, *2D Mater.*, 2017, **4**, 025092.